Electronic supplementary materials *Mendeleev Commun.*, 2025, **35**, 484–486

Ordered and disordered zirconia-modified silica supports in diclofenac hydrodechlorination over palladium catalyst

Ekaterina S. Lokteva, Evelina G. Khachatryan, Mikhail D. Pesotskiy, Elena V. Golubina, Konstantin I. Maslakov, Igor Yu. Kaplin, Sergey I. Kirikov and Sergey V. Maksimov

1. Background of this study

Chlorinated organic compounds are dangerous ecotoxicants that are highly resistant to biodegradation.[S1] They include many pharmaceuticals, such as the non-steroidal anti-inflammatory drug diclofenac (DCF).[S2] Throughout its life cycle DCF migrates into the environment, contaminating ground and drinking water. Conventional water treatment plants are very poor at removing DCF. More promising is its reductive dechlorination, or hydrodechlorination. This reaction converts DCF into 2-(2-anilinophenyl)acetate which has a maximum allowable concentration about five times higher than that of DCF.[S3] Previously, a number of studies have demonstrated the high efficiency of palladium catalysts in the hydrodechlorination of chlorophenol[S4] and DCF[S5] in aqueous media.

The efficiency of palladium catalyst strongly depends on the chemical nature and textural properties of the support. A high specific surface area of the support promotes high dispersion of palladium particles, while its chemical nature affects the acidic properties of the surface, the oxidation state of palladium, its reducibility, *etc.* Alumina is the most used catalyst support for DCF conversion.[S5–S7] Silica,[S8] zirconia[S9] and zeolytes[S10] are also efficient supports of Pd catalysts for DCF hydrodechlorination.

Partially oxidized palladium ($Pd^{\delta+}$), which can activate the C−Cl bond is favorable for high hydrodechlorination activity of the catalyst.[S11] This effect is more pronounced for electron-deficient small nanoparticles and clusters that donate electron density to the support. The high reactivity and even higher stability of small palladium nanoparticles than those of large ones were observed in the hydrodechlorination of trichloroethylene in aqueous medium.[S12] The pore size limits the size of palladium particles synthesized in the pores of the support. Recently, in the hydrodechlorination of 2,4,6-trichloroanisole in an aqueous medium, the increased efficiency of palladium catalysts obtained by the ion-exchange method and containing palladium particles predominantly in the pores of the zeolite was demonstrated in comparison with analogs obtained by impregnation of the same support.[S13] 2,4-Dichlorophenoxyacetic acid was successfully hydrodechlorinated over a composite catalyst comprising palladium nanoparticles and nitrogen-doped carbon quantum dots (d-NCQD) located in the pores of ordered mesoporous SBA-15 silica.[S14]

Mild reduction conditions of palladium particles are highly desirable to prevent their sintering and make the treatment cost effective. Previously, it has been shown that Pd^{2+} supported on Al_2O_3, ZrO_2 and disordered mesoporous ZrO_2–SiO_2 (hereinafter referred to as ZS) can be reduced to some extent with hydrogen even under very mild conditions (30 °C, aqueous suspension), *i.e.*, actually under the reaction conditions.[S9,S15] The low temperature treatment is important to increase the stability of the catalyst against deactivation during chlorination by HCl released during the reaction and to prevent sintering of small palladium particles, which is more likely to occur during high temperature reduction. The ability of

supported PdO particles to undergo mild reduction depends on the nature and textural properties of the support.

X-ray photoelectron spectroscopy (XPS) revealed the migration of palladium from the surface into the bulk of the Al_2O_3 and ZS supports under high-temperature reduction.[S7] Ordered mesoporous supports can effectively prevent palladium depletion from the catalyst surface during the preparation stage.

2. Preparation of the carriers and supports.

The zirconia-modified SBA-15 mesoporous silica support (ZrSBA) with ordered mesopores was synthesized by co-precipitation from zirconium oxynitrate (99.5%, Acros Organics, Belgium) and tetraethoxysilane (TEOS) (high purity, Component-reaktiv, Russia) using hydrolysis under thermal-vapor conditions (in an autoclave) as described previously.[S16] Pluronic P-123 (Sigma-Aldrich, USA) was used as a template, and pentaerythritol (RusChem, Russia) was used as a masking ligand to slow down the hydrolysis of the zirconium salt. The Si/Zr molar ratio was 92 : 8. The support was calcined in two stages: firstly, it was slowly heated to 250 °C and held for 3 h, and then heated to 500 °C and held at this temperature for 3 h.

The disordered mesoporous ZrO_2–SiO_2 (ZS) support was prepared as described previously.[S7] The Si/Zr molar ratio was 55 : 45. The support was calcined at 500 °C.

Palladium was applied by wet impregnation of the supports with a palladium nitrate solution (pure, JSC 'Aurat', Moscow, Russia) followed by drying and calcination at 500 °C (4 h). Before catalytic tests the catalysts were reduced for 2 h in two ways: (1) at 320 °C in H_2 flow in a fixed bed quartz tubular reactor followed by passivation in N_2 flow with an admixture of O_2 [these catalysts are designated as Pd/ZS(320) and Pd/ZrSBA(320)] and (2) at 30 °C by bubbling H_2 through a suspension of catalyst precursor in 15 ml of distilled water with stirring in a batch reactor [such reduced catalysts are designated as Pd/ZS(30) and Pd/ZrSBA(30)].

When depositing palladium on an ordered mesoporous support, we deliberately reduced the palladium content to minimize the cost of the catalyst and the pore closure by the palladium particles. To improve the reliability of data comparison for catalysts with different palladium contents, we carefully determined the true bulk palladium loading by AAS.

3. Physical-chemical studies of the catalysts.

The palladium content in the samples (Table 1, see the main article) was determined by AAS (Thermo Fisher Scientific iCE 3000 series, Thermo Scientific, USA, air/acetylene flame atomizer, processing with the SOLAAR Data Station software) after dissolution in a mixture of acids (HF and HNO_3 for Pd/ZrSBA, HCl and HNO_3 for Pd/ZS). The palladium loading was approximately 9 times higher in Pd/ZS.

Low-temperature nitrogen physisorption isotherms of the catalysts were recorded using Autosorb–1 (Quantachrome, USA) after calcination of the samples (ZrSBA and Pd/ZrSBA for 9 h at 200 °C, ZS and Pd/ZS for 3 h at 200 °C).

Small angle X-ray diffraction (PANalytical X'Pert Pro diffractometer with $CuK\alpha_{1/2}$ radiation and PIXcel detector equipped with a graphite monochromator) data were registered in air in the 2θ angular interval of 0.4–4.0° with a step size of 0.026° and Δt of 200 s per step.

XRD patterns were recorded using MiniFlex 300/600 diffractometer (Rigaku, Tokyo, Japan) at CuKα radiation of 1.5418 Å. Processing of the obtained results using the Scherrer formula gave a very rough estimate of the palladium particle size (peak at $2\theta = 40°$), which was 8 nm for Pd/ZS and 10 nm for Pd/ZrSBA.

TEM study was performed on JEM 2100F-UHR instrument equipped with EDA accessory (JEOL, Tokyo, Japan) with accelerating voltage of 200 kV.

XPS spectra were recorded on Axis Ultra DLD spectrometer (Kratos Analytical, UK) with monochromatic AlK_α source ($h\nu$ = 1486.7 eV, 150 W). The pass energies of the analyzer were 160 eV for survey spectra and 40 eV for high resolution scans. The binding energy scale of the spectrometer was preliminarily calibrated using the position of the peaks for the Au $4f_{7/2}$ (83.96 eV), Ag $3d_{5/2}$ (368.21 eV) and Cu $2p_{3/2}$ (932.62 eV) core levels of pure metallic gold, silver and copper, respectively. The Kratos charge neutralizer system was used. The high-temperature reduction of the catalysts pressed in tablets was carried out *in situ* in the catalytic cell of the spectrometer with a mixture of 5 vol% H_2 + + 95 vol% Ar. Prior to reduction, these tablets were employed for the recording of the spectra of non-reduced catalysts. The low-temperature reduction was the same as before the catalytic tests; the reduced powders were dried in a hydrogen flow and immediately transferred to the XPS analysis in a closed vial under hydrogen atmosphere.

TPR experiments were performed on USGA-101 chemisorption analyzer (Unisit, Russia). After the pre-treatment in Ar for 0.5 h at 300 °C, TPR profiles recorded in a flow of 5% H_2 + 95% Ar (30 ml min^{-1}) with heating from 30 to 850 °C at a rate of 10 °C min^{-1}.

4. Catalytic tests and the analysis of products.

The catalysts (0.05 g) were tested at 30 °C in a batch reactor in the water solution of DCF (150 mg dm^{-3}, 15 ml) stirred with a magnetic stirrer under supplying 0.6 dm^3 h^{-1} of pure H_2. The samples were periodically taken from the reactor without stopping stirring, centrifuged to separate the catalyst and analyzed by HPLC (Agilent 1100 Series instrument, Agilent Technologies Inc., USA) using a Zorbax SB-C18 column (15 cm) at 35 °C and a UV-detector at 278 nm. A mixture of 0.1 M formic acid and acetonitrile (1 : 1, vol/vol) was used as an eluent.

TOF values were calculated using the equation:

$$\mathrm{TOF} = \frac{\Delta C(\mathrm{DCF})}{\Delta t \times m(\mathrm{Pd})},$$

where ΔC(DCF) is the change in the DCF concentration in the initial linear part of the conversion versus time curve, Δt is the duration of this part, m(Pd) is the mass of palladium in the catalyst sample.

Table S1 Texture properties of the samples from N_2 adsorption results.

Catalyst	Pd (wt%)[a]	Zr/Si (at/at)	S_{BET}/ $m^2\ g^{-1}$	BJH (adsorption branch)		DFT (adsorption branch)	
				d_{pore}/nm	V_{pore},/$cm^3\ g^{-1}$	d_{pore}/nm	V_{pore}/$cm^3\ g^{-1}$
Pd/ZS	0.86	0.818	340 ± 34	5.6	0.34	6.1	0.37
Pd/ZrSBA	0.10	0.087	610 ± 60	7.4	0.56	7.0	0.66

[a] AAS data.

Table S2 H_2 uptake for the reduction of PdO to Pd^0 calculated from AAS data and experimental H_2 release for the decomposition of PdH_x to Pd^0 calculated from the negative peak in the TPR profiles of the catalysts.

Catalyst	Amount of H_2/μmol g_{cat}^{-1}		Amount of H_2/μmol g_{Pd}^{-1}	
	$PdO \rightarrow Pd^0$ uptake	$PdH_x \rightarrow Pd^0$ release	$PdO \rightarrow Pd^0$ uptake	$PdH_x \rightarrow Pd^0$ release
Pd/ZrSBA	9.4	170	940	1700
Pd/ZS	81	83	94	97

Comment on Table S2. It can be seen that palladium in the Pd/ZrSBA composition absorbs significantly more hydrogen per unit weight than in the Pd/ZS composition. The amount of hydrogen released during the decomposition of palladium hydride is particularly different. For Pd/ZrSBA this amount is several orders of magnitude higher than for Pd/ZS. These data confirm the presence of relatively large palladium particles capable of forming the palladium hydride phase.

Table S3 Zr/Si ratios determined in the bulk and on the surface of catalysts before and after reduction under mild and severe conditions.

Catalyst	Zr/Si (at/at)	
	Bulk (based on synthesis method)	Surface (calculated from XPS data)
Pd/ZS	0.818	0.085
Pd/ZS(30)		0.477
Pd/ZS(320)		0.083
Pd/ZrSBA	0.087	0.059
Pd/ZrSBA(30)		0.056
Pd/ZrSBA(320)		0.058

Comment on Table S3. It can be seen that for all the efficient catalysts the Zr/Si surface ratio is similar and small, despite the difference in bulk values for Pd/ZS and Pd/ZrSBA. Only for the least active Pd/ZS(30) is it sufficiently large and close to the bulk ratio. The encapsulation of Pd with Zr may be one of the reasons for the low activity of this sample.

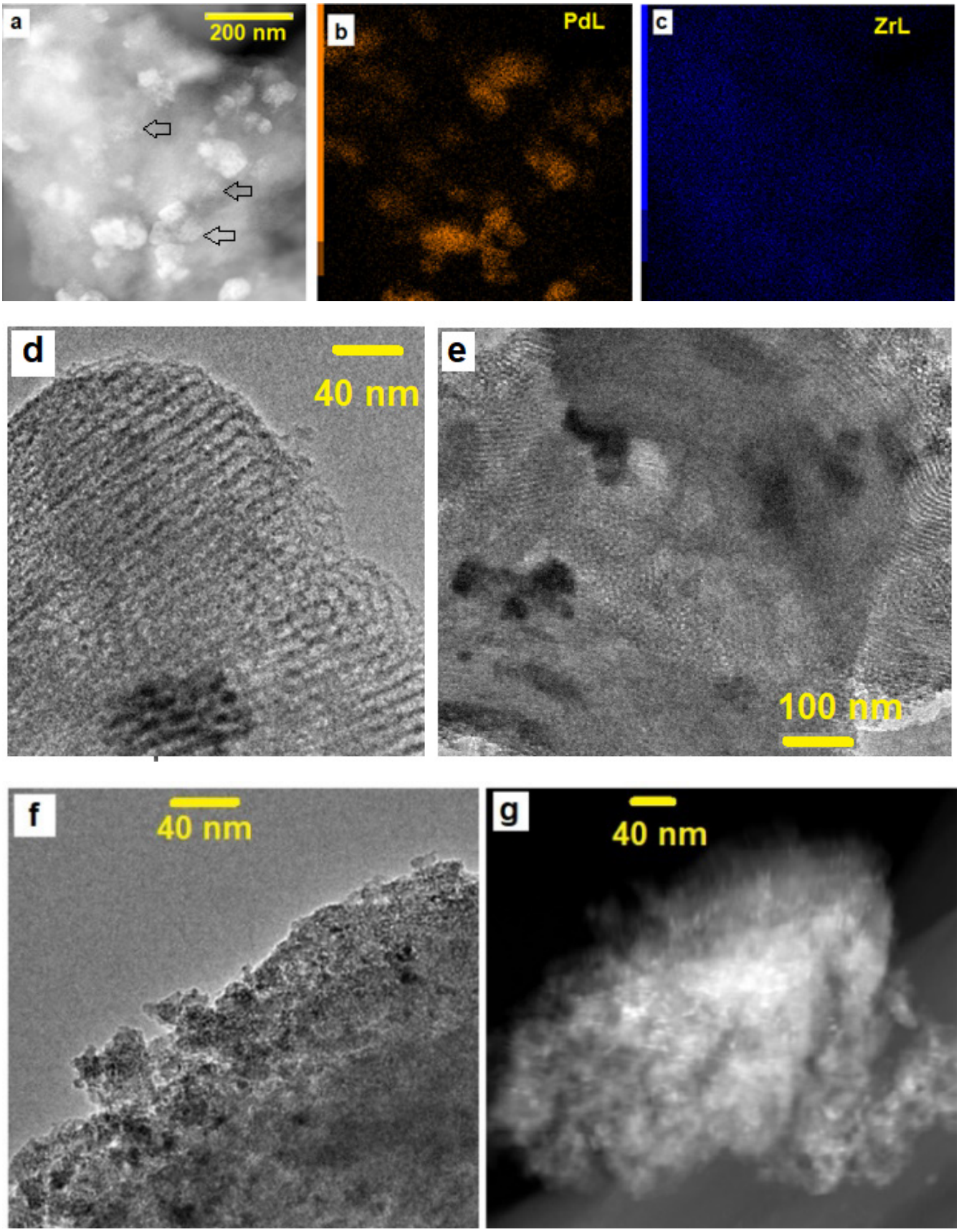

Figure S1 (*a*) STEM image of Pd/ZrSBA(320); (*b*, *c*) EDA elemental mapping of PdL and ZrL for image (*a*); (*d*, *e*) bright field TEM images of Pd/ZrSBA(320); (*f*, *g*) bright field and dark field TEM images of Pd/ZS.

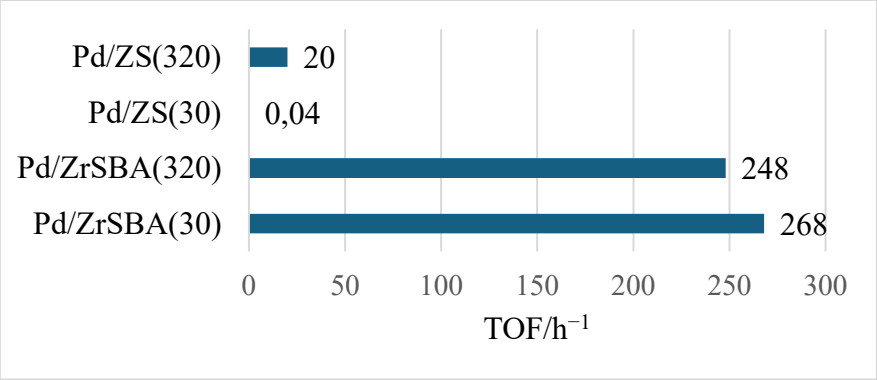

Figure S2 TOF values for hydrodechlorination of DCF over Pd catalysts. Conditions: 0.05 g of catalyst, C_0(DCF) = 150 mg dm^{-3}, 30 °C, pH 7, 0.6 dm^3 h^{-1} of H_2.

References

S1 E. Lokteva, E. Golubina, V. Likholobov and V. Lunin, in *Chemistry Beyond Chlorine*, eds. P. Tundo, L.-N. He, E. Lokteva and C. Mota, Springer, Cham, 2016, pp. 559–584; https://doi.org/10.1007/978-3-319-30073-3_21.

S2 J. Schwaiger, H. Ferling, U. Mallow, H. Wintermayr and R. D. Negele, *Aquat. Toxicol.*, 2004, **68**, 141; https://doi.org/10.1016/j.aquatox.2004.03.014.

S3 L. Lonappan, S. K. Brar, R. K. Das, M. Verma and R. Y. Surampalli, *Environ. Int.*, 2016, **96**, 127; https://doi.org/10.1016/j.envint.2016.09.014.

S4 E. S. Lokteva, V. V. Shishova, N. N. Tolkachev, K. I. Maslakov, A. O. Kamaev, S. V. Maksimov, and E. V. Golubina, *Mendeleev Commun.*, 2022, **32**, 249; https://doi.org/10.1016/j.mencom.2022.03.032.

S5 J. Nieto-Sandoval, M. Munoz, Z. M. de Pedro and J. A. Casas, *J. Hazard. Mater.*, 2022, **5**, 100047; https://doi.org/10.1016/j.hazadv.2022.100047.

S6 J. Nieto-Sandoval, M. Munoz, Z. M. de Pedro and J. A. Casas, *Sep. Purif. Technol.*, 2019, **227**, 115717; https://doi.org/10.1016/j.seppur.2019.115717

S7 E. S. Lokteva, V. V. Shishova, K. I. Maslakov, E. V. Golubina, A. N. Kharlanov, I. A. Rodin, M. F. Vokuev, D. S. Filimonov and N. N. Tolkachev, *Appl. Surf. Sci.*, 2023, **613**, 156022; https://doi.org/10.1016/j.apsusc.2022.156022.

S8 K. Wu, X. Qian, L. Chen, Z. Xu, S. Zheng and D. Zhu, *RSC Adv.*, 2015, **5**, 18702; https://doi.org/10.1039/c4ra16674d.

S9 V. V. Shishova, E. S. Lokteva, G. S. Maksimov, K. I. Maslakov, I. Yu. Kaplin, S. V. Maksimov and E. V. Golubina, *Moscow Univ. Chem. Bull.*, 2024, **79**, 156; https://doi.org/10.3103/S0027131424700123.

S10 B. Zawadzki, E. Kowalewski, M. Asztemborska, K. Matus, S. Casale, S. Dzwigaj and A. Śrębowata, *Catal. Commun.*, 2020, **145**, 106113; https://doi.org/10.1016/j.catcom.2020.106113.

S11 N. S. Babu, N. Lingaiah, N. Pasha, J. V. Kumar and P. S. S. Prasad, *Catal. Today*, 2009, **141**, 120; https://doi.org/10.1016/j.cattod.2008.03.018.

S12 S. Karahan and G. Celik, *J. Environ. Chem. Eng.*, 2024, **12**, 112467; https://doi.org/10.1016/j.jece.2024.112467.

S13 Y. Zhang, P. Ma, H. Fu, X. Qu and S. Zheng, *Chemosphere*, 2022, **309**, 136551; https://doi.org/10.1016/j.chemosphere.2022.136551.

S14 H. Liu, L. Long, Z. Xu and S. Zheng, *Chem. Eng. J.*, 2020, **400**, 125987; https://doi.org/10.1016/j.cej.2020.125987.

S15 E. S. Lokteva, M. D. Pesotskiy, E. V. Golubina, K. I. Maslakov, A. N. Kharlanov, V. V. Shishova, I. Yu. Kaplin and S. V. Maksimov, *Kinet. Catal.*, 2024, **65**, 133; https://doi.org/10.1134/S0023158423601183.

S16 T. Qiang, J. Zhao and J. Li, *Microporous Mesoporous Mater.*, 2018, **257**, 162; https://doi.org/10.1016/j.micromeso.2017.08.041.